DOI 10.15622/ia.24.1.4

T. MUSLIMOV

COLLISION AVOIDANCE IN CIRCULAR MOTION OF A FIXED-WING DRONE FORMATION BASED ON ROTATIONAL MODIFICATION OF ARTIFICIAL POTENTIAL FIELD

Muslimov T. **Collision Avoidance in Circular Motion of a Fixed-Wing Drone Formation Based on Rotational Modification of Artificial Potential Field.**

Abstract. In coordinated circular motion of a group of autonomous unmanned aerial vehicles (UAVs or drones), it is important to ensure that collisions between them are avoided. A typical situation occurs when one of the drones in circular formation needs to overtake the drone ahead. The reason for such an overtake may be due to a given geometry of the UAV formation, when this configuration of a given relative position of the drones has changed for some reason. In this case, the limited maneuverability of UAVs of exactly fixed-wing type requires taking into account the peculiarities of their dynamics in the synthesis of the collision avoidance algorithm. The impossibility of the airspeed for a fixed-wing type UAV to drop below a certain minimum value also plays a role here. In this paper, we propose to use an approach based on vortex vector fields, which are essentially a rotational modification of the artificial potential field (APF) method. In this case, the path following algorithm developed in our previous works provides the circular motion. As a result, a collision avoidance algorithm has been developed that works efficiently by maintaining coordinated circular motion of the autonomous drone formation without unnecessary turns. The proposed algorithm was named Artificial Potential Field for Circular Motion (abbreviated as APFfCM). Using the direct Lyapunov method, it is shown that the trajectories of the formation system have uniform boundedness (UB) when using the proposed control algorithm. Due to the boundedness of the candidate Lyapunov function, it is guaranteed that no collision event between drones will occur. Thus, the control objective of providing coordinated circular motion for an autonomous fixed-wing type drone formation without collisions is achieved. Fixed-wing ("flying wing") UAV models in MATLAB/Simulink environment demonstrate the effective performance of the proposed algorithm. These models have both full nonlinear dynamics and implementation of tuned autopilots stabilizing angular and trajectory motion.

Keywords: collision avoidance, drone teams, multi-UAV system, artificial potential field method, vortex vector field.

1. Introduction. The artificial potential field (APF) method [1, 2] has been widely developed for various types of robots: both industrial manipulators and mobile types. From its basic version, this approach has received in its development many modifications, for the possibilities of use in specific models of controlled objects. For example, significantly modified APF methods have been used for high-level models in the form of a double integrator [3], as well as for wheeled mobile robots [4-7]. However, the use of the APF method on unmanned aerial vehicles (UAVs or drones) has its limitations [8]. This is especially evident in the case of fixed-wing type drones, which have limited maneuverability due to nonholonomic dynamics.

A rotationally modified vector field-based APF (vortex vector field) method for motion planning and collision avoidance in robot control was

probably first proposed and studied in detail in [9, 10]. This approach was further developed for mobile robots [11]. The application of rotational vector field for mobile robots avoiding collisions on an opposite course was studied in [12]. In [13], a strategy for avoiding collisions between two UAVs while moving on an opposite course is considered. In [14], this concept was applied to a single quadrocopter avoiding a collision with a fixed obstacle. In [15], fuzzy logic theory and genetic algorithm are used to further modify such an improved potential field. In [16, 17], the rotational modification of the potential field is successfully applied to a single quadrocopter and a stationary obstacle. In [18], a new modified algorithm based on the vortex vector field is developed to enable a wheeled mobile robot to effectively avoid collision with a stationary obstacle. The main advantage of the vortex vector field can be described as the efficient escape of the robot from the local minimum state, the simplicity of the algorithm tuning, and the insignificant influence of the evasive maneuver on the final performance of the main mission. In the case of circular formation motion performed while tracking some object, this strategy should be significantly modified. The special feature here is that the UAVs must not only evade the collision, but also successfully return to the circular motion orbit.

In [19], a rotational modification of the artificial potential field is applied to the formation of quadrocopters, but the stability preservation of such a modification has not been analyzed. In [20], the application of rotational modification for the artificial potential field in controlling a group of rotary-wing drones was discussed. The paper [21] also studied the motion of rotary-wing type drone models jointly avoiding collision with a stationary obstacle. However, this study has the following significant differences from [20, 21]: first, the application of the modification on fixed-wing type UAVs has additional complexity due to the limited maneuverability of this type of aircraft; second, it is the circular motion that is studied here, which imposes certain requirements for maintaining the consistency of the group's flight. Some papers propose strategies similar to the vortex vector field, e.g., [22] uses an orthogonal component that shifts the robot from a local minimum state. However, this approach is fundamentally different in the way the control algorithm is designed.

Let us consider in more detail the difference between this paper and our previous one. In [20] a special vector $\mathbf{f}^{escape}(\mathbf{q}_i, \mathbf{q}_{i+1})$ was used:

$$\mathbf{f}^{escape}(\mathbf{q}_i, \mathbf{q}_{i+1}) \triangleq \mu_i (\mathbf{q}_i - \mathbf{q}_{i+1}) / \|\mathbf{q}_i - \mathbf{q}_{i+1}\|_2^2,$$

where μ_i is an adjustable positive coefficient; $\mathbf{q}_i$ and $\mathbf{q}_{i+1}$ are the vectors of UAV positions numbered i and $i+1$ in the global coordinate system. The UAVs

under these numbers must perform collision avoidance. A "danger zone" is introduced as a region of flight space within which the potential repulsion field starts to operate. The radius of this region is denoted as d_o ("safety radius"). The vector $\mathbf{f}^{escape}(\mathbf{q}_i, \mathbf{q}_{i+1})$ allows a pair of UAVs to leave the "danger zone" and continue circular motion according to the original mission.

If we consider $\|\mathbf{q}_i - \mathbf{q}_{i+1}\|_2 = d_o$ as the equilibrium position for the nominal system (not using $\mathbf{f}^{escape}(\mathbf{q}_i, \mathbf{q}_{i+1})$ in the control algorithm), then $\mathbf{f}^{escape}(\mathbf{q}_i, \mathbf{q}_{i+1})$ is a non-vanishing perturbation. Note an important point: it is not shown in [20] that the equilibrium position $\|\mathbf{q}_i - \mathbf{q}_{i+1}\|_2 = d_o$ is Lyapunov stable (in contrast to the equilibrium positions of the formation after leaving the "danger zone"). Moreover, it can be easily shown that $\|\mathbf{q}_i - \mathbf{q}_{i+1}\|_2 = d_o$ is Lyapunov unstable (e.g., using Chetaev's theorem). However, it was found in [20] that in the region $\|\mathbf{q}_i - \mathbf{q}_{i+1}\|_2 \leqslant d_o$ the derivative of the candidate Lyapunov function (denoted as V) is nonpositive. This fact means that the candidate Lyapunov function V is decreasing in the region $\|\mathbf{q}_i - \mathbf{q}_{i+1}\|_2 \leqslant d_o$, that is, $V(t) \leqslant V(0)$. In practical terms, it follows that two quadrocopters placed inside the region $\|\mathbf{q}_i - \mathbf{q}_{i+1}\|_2 \leqslant d_o$, but not at the collision point $\|\mathbf{q}_i - \mathbf{q}_{i+1}\|_2 = 0$, will not hit this collision point at subsequent times. This is justified by the fact that at the collision point $\|\mathbf{q}_i - \mathbf{q}_{i+1}\|_2 = 0$ candidate Lyapunov function tends to plus infinity, which contradicts the condition $V(t) \leqslant V(0)$. Thus, we explained that the component $\mathbf{f}^{escape}(\mathbf{q}_i, \mathbf{q}_{i+1})$ was introduced specifically to destabilize the nominal system that uses only the artificial potential field-based algorithm. This destabilization allows drones performing collision avoidance to successfully leave the "danger zone" in a finite amount of time.

In our current study, the original mission is the coordinated circular motion of the team. Therefore, instead of the vector $\mathbf{f}^{escape}(\mathbf{q}_i, \mathbf{q}_{i+1})$, an additional vector field component is applied to follow the circular path in combination with a rotational modification of the vector field. This additional component can also be considered as a non-vanishing perturbation for a nominal system that uses only the vector field component derived from the artificial potential field.

Thus, the main contribution of this paper is as follows:

– a rotational modification of the artificial potential field (vortex vector field) is considered specifically for autonomous fixed-wing drones, and in the problem of circular coordinated motion;

– using the direct Lyapunov method, the stability of the equilibrium is analyzed; the uniform boundedness (UB) of the trajectories (so-called Lagrange stability) guarantees that no collision event will occur;

– the proposed algorithm is simulated on full nonlinear models of fixed-wing type UAVs; the obtained results clearly illustrate the efficiency of the proposed algorithm.

2. Collision avoidance algorithm for a group of fixed-wing type drones. Consider the motion of two fixed-wing type UAVs in a formation making a circular motion. In this case, UAV No.$(i+1)$ is ahead of UAV No.i in a circular orbit. However, according to the formation control algorithm, the UAV No.i should be ahead of the UAV No.$(i+1)$ at a predetermined distance in steady-state. If the collision avoidance algorithm is not applied, a collision will occur between the two UAVs as UAV No.i will try to overtake UAV No.$(i+1)$ while traveling in a circular orbit.

Objectives: when automating the flight of a circular formation of small UAVs on the basis of decentralized interaction, it is necessary to prevent collisions between drones in a group while maintaining the specified flight altitude by each of the vehicles. In this case, circular motion is based on the path following algorithm in autonomous mode, that is, the drones autonomously execute the embedded control algorithm. A specific technical realization of autonomous circular formation can be based on ZigBee [23] or a mesh network using 900 MHz RF modems [24]. The collision avoidance algorithm should be developed specifically for the above-described flight mode of the drone formation.

Next, we consider the main modifications of the standard artificial potential field (APF) algorithm that lead to the collision avoidance algorithm proposed in this paper. The first modification of the standard APF algorithm: the Attractive Potential Field is not used in the algorithm. Instead of this field, a Path Following Vector Field is used, which is generated by the formation control algorithm for circular motion.

The second modification compared to the work of [20]: no rotationally modified vector field (zero-rotor in this case) is applied for the UAV ahead (in this case, it is UAV No.$(i+1)$). The reason for this is that, due to the limited maneuverability of the fixed-wing drone, the application of a rotationally modified vector field causes the drone to undesirably turn completely around. At the same time, UAV No.$(i+1)$ will also deviate significantly from the basic circular motion trajectory following UAV No.i, since the rotationally modified vector field assumes a circular trajectory around the obstacle. This problem is illustrated in Figure 1, which shows the motion trajectories when using the vector field with rotational modification on both UAV No.i and UAV No.$(i+1)$. This illustration clearly demonstrates the inefficiency of using the rotationally modified vector field for UAV No.$(i+1)$.

The third modification: for a UAV using a vortex vector field, an additional condition is imposed to turn off the evasive maneuver if it overtakes a UAV flying ahead. The overtaking event can be defined by computing the triple product of the vectors: $T_{prod} = \mathbf{n} \cdot (\mathbf{d}_i \times \mathbf{d}_{i+1})$, where $\mathbf{n} = \begin{bmatrix} 0, & 0, & 1 \end{bmatrix}^{\mathrm{T}}$, and $\mathbf{d}_*$ is the distance vector from the center of the circular path to the UAV with the lower index corresponding to the ordinal number of the UAV in the formation. If $T_{prod} < 0$, this means that UAV No.i is behind UAV No.$(i+1)$ and will try to overtake it. The value $T_{prod} > 0$ will mean that the overtaking has already occurred. Note that switching off the evasive maneuver should not be done immediately after overtaking, but after reaching a certain distance (this is shown later in the control algorithm).

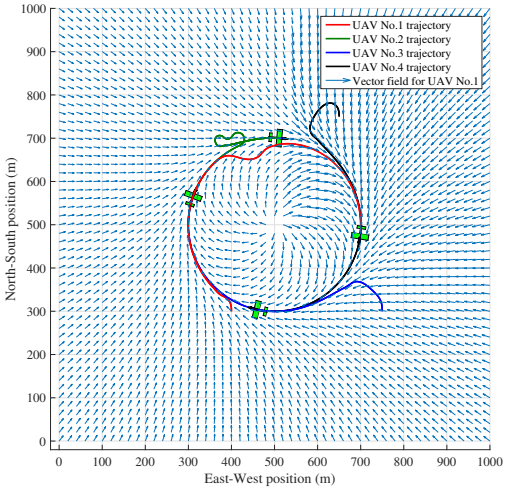

Fig. 1. Trajectories of fixed-wing type UAVs using a vector field with rotational modification

The complete potential field-based collision avoidance algorithm designed for circular motion of UAV formation (we named "Artificial Potential Field for Circular Motion" – APFfCM) is as follows. First, the ordinal numbers of the “overtaking” (No.i) and “overtaken” (No.$(i+1)$) UAVs on the circular path are determined. For this purpose, the triple product $T_{prod} = \mathbf{n} \cdot (\mathbf{d}_i \times \mathbf{d}_{i+1})$ sign should be used. In this case, it is important how exactly this value is calculated initially. The order of the product in brackets plays a role in the expression $\mathbf{n} \cdot (\mathbf{d}_i \times \mathbf{d}_{i+1})$, i.e. which UAV is selected as the i-th and which as

the $(i+1)$-th. In the formation control algorithm, it is assumed that the current angle between the UAVs is given by the center angle α when computing T_{prod}, so the value of this angle is assumed to be less than or equal to π radians. However, also initially the angle can be given through the value of $2\pi - \alpha$, and this should be provided in the structure of the formation control algorithm itself.

Thus, in order to determine the correct order or disorder in the formation, it is necessary to know the inherent rule for determining the angles. For example, for a formation of three UAVs, the inherent rule that the center angle should not exceed π radians makes sense. Therefore, it will be considered that the UAV number i is ahead of the UAV number $i+1$ if $T_{prod} > 0$. Otherwise, the order will be broken and the UAV number i will try to overtake the UAV number $i+1$. As a result, without a collision avoidance algorithm, a collision between UAVs may occur.

Figure 2 on the left shows that if the algorithm is applied to a formation of two UAVs, the originally laid down method of angle calculation can be changed during flight so that overtaking will not occur, since the UAV number $i+1$ can move to a given position by making a turn in an arc of greater length. However, as can be seen from Figure 2 on the right, such a change in the embedded method is no longer possible in the case of a formation of three or more UAVs, because in this case, the UAV number $i+1$ will meet the UAV number $i+2$ on its way (and the rest when the number of UAVs in the formation increases, due to which the number of required obstacle avoidance maneuvers becomes larger than in case of exchanging places of vehicles with numbers i and $i+1$). Therefore, there is a need to develop a collision avoidance algorithm for a decentralized formation of UAVs making such a circular motion.

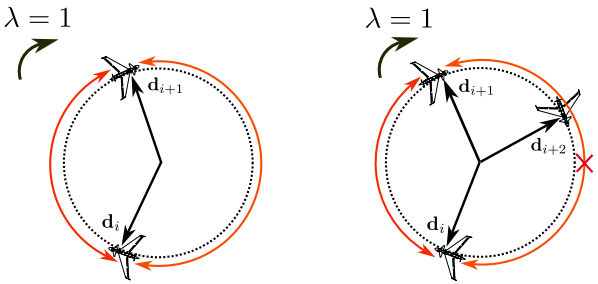

Fig. 2. Disorder in the formation of UAVs

A high-level model of an autopilot-stabilized UAV is considered as

$$\begin{aligned} \mathbf{q}_i &= \begin{bmatrix} p_i^e, & p_i^n \end{bmatrix}^{\mathrm{T}}, \\ \dot{\mathbf{q}}_i &= \begin{bmatrix} v_i \sin\psi_i, & v_i \cos\psi_i \end{bmatrix}^{\mathrm{T}}, \end{aligned} \tag{1}$$

where p_i^e is the position along the coordinate axis pointing East (east axis); p_i^n is the position along the coordinate axis pointing North (north axis); v_i is the airspeed; ψ_i is the course. These states according to the lower index refer to UAV No.i. In this case, the course is measured from the north axis.

Let us define the repulsive artificial potential field (APF) function in the following form of the classical artificial potential, in this case the FIRAS function was chosen [2]:

$$U_r^{\mathrm{APFfCM}}(\mathbf{q}_i, \mathbf{q}_{i+1}) = \begin{cases} \frac{1}{2} k_{r_i} \left(\frac{1}{d(\mathbf{q}_i, \mathbf{q}_{i+1})} - \frac{1}{d_o} \right)^2, & \text{if} \quad d(\mathbf{q}_i, \mathbf{q}_{i+1}) \leqslant d_o; \\ 0, & \text{if} \quad d(\mathbf{q}_i, \mathbf{q}_{i+1}) > d_o, \end{cases} \tag{2}$$

where constant coefficient $k_{r_i} \in \mathbb{R}_{>0}$;
$d(\mathbf{q}_i, \mathbf{q}_{i+1})$ is the distance between UAV No.i and UAV No.$(i+1)$;
d_o is the radius of the so-called "danger zone" within which the action of the potential field of repulsion begins.

Since the UAVs are on the same path line during the circular motion, applying only the standard artificial potential field on both UAVs performing the evasive maneuver may cause a local minimum effect. For this reason, the repulsive artificial potential field for the algorithm is proposed as a function of the artificial potential with rotational modification.

Next, for UAV No.i, we specify the component $\mathbf{f}_r^i(\mathbf{q}_i, \mathbf{q}_{i+1}) \in \mathbb{R}^2$ used in the control law and defined by multiplying the gradient with the opposite sign of the repulsive potential field U_r^{APFfCM} (2) by the rotation matrix $\mathbf{R}(\lambda)$. Thus, we can obtain:

$$\begin{aligned} &\mathbf{f}_r^i(\mathbf{q}_i, \mathbf{q}_{i+1}) = \\ &= -\nabla U_r^{\mathrm{APFfCM}}(\mathbf{q}_i, \mathbf{q}_{i+1}) \mathbf{R}(\lambda) \\ &= \begin{cases} k_{r_i} \left(\frac{1}{d(\mathbf{q}_i, \mathbf{q}_{i+1})} - \frac{1}{d_o} \right) \frac{\mathbf{q}_i - \mathbf{q}_{i+1}}{d^3(\mathbf{q}_i, \mathbf{q}_{i+1})} \mathbf{R}(\lambda), & \text{if} \quad d(\mathbf{q}_i, \mathbf{q}_{i+1}) \leqslant d_o; \\ 0, & \text{if} \quad d(\mathbf{q}_i, \mathbf{q}_{i+1}) > d_o, \end{cases} \end{aligned} \tag{3}$$

where

$$\mathbf{R} = \begin{cases} \begin{bmatrix} 0 & 1 \\ -1 & 0 \end{bmatrix} & \text{if} \quad \lambda = -1 \Rightarrow \text{clockwise}, \\ \\ \begin{bmatrix} 0 & -1 \\ 1 & 0 \end{bmatrix} & \text{if} \quad \lambda = 1 \Rightarrow \text{counterclockwise}. \end{cases} \tag{4}$$

Let us clarify the role of the parameter λ in equation (4). In this case, it specifies the direction of rotation of the formation. The value $\lambda = 1$ indicates clockwise rotation of the formation (when viewed from above), in which case UAV No.i should perform the collision avoidance maneuver according to the vector field with counterclockwise rotational modification. Exactly such a choice of rotation is due to the fact that at some point in time UAV No.i starts to return to the circular motion trajectory. Accordingly, the total path traveled by UAV No.i will be less in the case of maneuvering along the inner region of the circular area bounded by the circumference of the formation flight path. Thus, UAV No.i will be faster to overtake UAV No.$(i+1)$, which in turn, in the final part of the return trajectory will move along an arc of greater length than UAV No.i.

The control algorithm atan2 $\left(\mathbf{f}_i^{\text{APFfCM}}[1]; \mathbf{f}_i^{\text{APFfCM}}[2]\right)$ for the course of UAV No.i is computed using (3) through the vector $\mathbf{f}_i^{\text{APFfCM}} \in \mathbb{R}^2$, defined finally in the following way as shown in Sub-algorithm 1.

if $d(\mathbf{q}_i, \mathbf{q}_{i+1}) \leqslant d_o$ and $T_{prod} < T_{tresh}$ **then**
$$\begin{aligned} \mathbf{f}_i^{\text{APFfCM}}(\mathbf{q}_i, \mathbf{q}_{i+1}) &= \mathbf{f}_r^i(\mathbf{q}_i, \mathbf{q}_{i+1}) + \eta_i \mathbf{f}^{VF}(\mathbf{q}_i) \\ &= -\nabla_{\mathbf{q}_i} U_r^{\text{APFfCM}}(\mathbf{q}_i, \mathbf{q}_{i+1})\, \mathbf{R}(\lambda) \\ &\quad + \eta_i \mathbf{f}^{VF}(\mathbf{q}_i) \end{aligned}$$
if $d(\mathbf{q}_i, \mathbf{q}_{i+1}) > d_o$ or $d(\mathbf{q}_i, \mathbf{q}_{i+1}) \leqslant d_o \wedge T_{prod} \geqslant T_{tresh}$ **then**
$$\mathbf{f}_i^{\text{APFfCM}}(\mathbf{q}_i, \mathbf{q}_{i+1}) = \mathbf{f}^{VF}(\mathbf{q}_i)$$
end

Listing 1. Sub-algorithm 1

The following notation is used here:
T_{tresh} is a positive parameter chosen in advance;
$\mathbf{f}^{VF}(\mathbf{q}_i)$ is a vector given by circular path following vector field, the essence of which is disclosed in [25, 26];
$\eta_i \in \mathbb{R}_{>0}$ is an adjustable coefficient, which should be chosen sufficiently small, as will be explained later.

For the sake of clarity, we show an expanded form of the course control algorithm for UAV No.i in the case of clockwise motion in Sub-algorithm 2 below.

$$
\begin{aligned}
&\textbf{if } d(\mathbf{q}_i,\mathbf{q}_{i+1}) \leqslant d_o \text{ and } T_{prod} < T_{tresh} \text{ then}\\
&\quad \chi_c^{APF_i} = \operatorname{atan2}\left(v_e^{APF_i}; v_n^{APF_i}\right), \text{ where}\\
&\quad v_e^{APF_i} = \eta_i \sin\chi_i^c - k_{r_i}\left(\frac{1}{d(\mathbf{q}_i,\mathbf{q}_{i+1})} - \frac{1}{d_o}\right)\frac{p_i^n - p_{i+1}^n}{d^3(\mathbf{q}_i,\mathbf{q}_{i+1})}\\
&\quad v_n^{APF_i} = \eta_i \cos\chi_i^c + k_{r_i}\left(\frac{1}{d(\mathbf{q}_i,\mathbf{q}_{i+1})} - \frac{1}{d_o}\right)\frac{p_i^e - p_{i+1}^e}{d^3(\mathbf{q}_i,\mathbf{q}_{i+1})}\\
&\textbf{if } d(\mathbf{q}_i,\mathbf{q}_{i+1}) > d_o \text{ or } d(\mathbf{q}_i,\mathbf{q}_{i+1}) \leqslant d_o \wedge T_{prod} \geqslant T_{tresh} \text{ then}\\
&\quad v_e^{APF_i} = \eta_{v_i}\sin\chi_i^c,\ v_n^{APF_i} = \eta_{v_i}\cos\chi_i^c\\
&\text{end}
\end{aligned}
$$

Listing 2. Sub-algorithm 2

The following notation is used here:
$v_e^{APF_i}$ is the control component along the east axis;
$v_n^{APF_i}$ is the control component along the north axis;
χ_i^c is the course command given by the path following vector field;
$\eta_{v_i} \in \mathbb{R}_{>0}$ is a coefficient that depends on the implementation of the path following algorithm.

The control algorithm for UAV No.$(i+1)$ course will eventually look as follows as in Sub-algorithm 3.

$$
\begin{aligned}
&\textbf{if } d(\mathbf{q}_i,\mathbf{q}_{i+1}) \leqslant d_o \text{ and } T_{prod} < T_{tresh} \text{ then}\\
&\quad \mathbf{f}_{i+1}^{\text{APFfCM}}(\mathbf{q}_{i+1},\mathbf{q}_i) = \mathbf{f}^{APF}(\mathbf{q}_{i+1},\mathbf{q}_i) + \eta_{i+1}\mathbf{f}^{VF}(\mathbf{q}_{i+1})\\
&\qquad\qquad = -\nabla_{\mathbf{q}_{i+1}} U_r^{\text{APFfCM}}(\mathbf{q}_{i+1},\mathbf{q}_i)\\
&\qquad\qquad + \eta_{i+1}\mathbf{f}^{VF}(\mathbf{q}_{i+1})\\
&\textbf{if } d(\mathbf{q}_i,\mathbf{q}_{i+1}) > d_o \text{ or } d(\mathbf{q}_i,\mathbf{q}_{i+1}) \leqslant d_o \wedge T_{prod} \geqslant T_{tresh} \text{ then}\\
&\quad \mathbf{f}_{i+1}^{\text{APFfCM}}(\mathbf{q}_{i+1},\mathbf{q}_i) = \mathbf{f}^{VF}(\mathbf{q}_{i+1})\\
&\text{end}
\end{aligned}
$$

Listing 3. Sub-algorithm 3

The following notation is used here:
$\mathbf{f}^{APF}(\mathbf{q}_{i+1},\mathbf{q}_i)$ is the gradient with the opposite sign of the chosen artificial potential function;
$\mathbf{f}^{VF}(\mathbf{q}_{i+1})$ is a vector similar to $\mathbf{f}^{VF}(\mathbf{q}_i)$, but chosen for the drone number $i+1$;
$\eta_{i+1} \in \mathbb{R}_{>0}$ is a coefficient similar to η_{i+1},but chosen for the drone number $i+1$.

For the sake of clarity, we show an expanded form of the course control algorithm for UAV No.$(i+1)$ in the case of clockwise motion in Sub-algorithm 4 below.

if $d(\mathbf{q}_i, \mathbf{q}_{i+1}) \leqslant d_o$ and $T_{prod} < T_{tresh}$ then

$$v_e^{APF_{i+1}} = \eta_{i+1} \sin \chi_{i+1}^c + k_{r_{i+1}} \left(\frac{1}{d(\mathbf{q}_i, \mathbf{q}_{i+1})} - \frac{1}{d_o} \right) \frac{p_{i+1}^e - p_i^e}{d^3(\mathbf{q}_i, \mathbf{q}_{i+1})}$$

$$v_n^{APF_{i+1}} = \eta_{i+1} \cos \chi_{i+1}^c + k_{r_{i+1}} \left(\frac{1}{d(\mathbf{q}_i, \mathbf{q}_{i+1})} - \frac{1}{d_o} \right) \frac{p_{i+1}^n - p_i^n}{d^3(\mathbf{q}_i, \mathbf{q}_{i+1})}$$

if $d(\mathbf{q}_i, \mathbf{q}_{i+1}) > d_o$ or $d(\mathbf{q}_i, \mathbf{q}_{i+1}) \leqslant d_o \wedge T_{prod} \geqslant T_{tresh}$ then

$$v_e^{APF_{i+1}} = \eta_{v_{i+1}} \sin \chi_{i+1}^c, \; v_n^{APF_{i+1}} = \eta_{v_{i+1}} \cos \chi_{i+1}^c$$

end

Listing 4. Sub-algorithm 4

The following notation is used here:
$v_e^{APF_{i+1}}$ is the control component along the east axis;
$v_n^{APF_{i+1}}$ is the control component along the north axis;
$\chi_c^{APF_{i+1}}$ is the course command given by the path following vector field;
$k_{r_{i+1}} \in \mathbb{R}_{>0}$ is an adjustable constant coefficient;
$\eta_{v_{i+1}} \in \mathbb{R}_{>0}$ is a coefficient that depends on the implementation of the path following algorithm.

Let us denote "$d(\mathbf{q}_i, \mathbf{q}_{i+1}) \leqslant d_o$ and $T_{prod} < T_{tresh}$" as Condition 1 and "$d(\mathbf{q}_i, \mathbf{q}_{i+1}) > d_o$ or $d(\mathbf{q}_i, \mathbf{q}_{i+1}) \leqslant d_o \wedge T_{prod} \geqslant T_{tresh}$" as Condition 2.

The control sub-algorithm for absolute values of UAV velocities (i.e., speeds) is proposed as follows (v_i^c for No.i and v_{i+1}^c for No.$(i+1)$):

$$\begin{aligned} v_i^c &= \begin{cases} \left(\left[v_e^{APF_i} \right]^2 + \left[v_e^{APF_i} \right]^2 \right)^{1/2}, & \text{if Condition 1;} \\ v_{VF_i}^c, & \text{if Condition 2,} \end{cases} \\ v_{i+1}^c &= \begin{cases} \left(\left[v_e^{APF_{i+1}} \right]^2 + \left[v_e^{APF_{i+1}} \right]^2 \right)^{1/2}, & \text{if Condition 1;} \\ v_{VF_{i+1}}^c, & \text{if Condition 2.} \end{cases} \end{aligned} \tag{5}$$

In this case, it is necessary to set speed limits in the control algorithm itself, taking into account the peculiarities of fixed-wing UAV dynamics:

$$v_i^c \in [v_{\min}; v_{\max}] \wedge v_{i+1}^c \in [v_{\min}; v_{\max}].$$

The following notation is used here:
$v_{\max}$ is the selectable maximum speed value;
$v_{\min}$ is the selectable minimum speed value;

$v^c_{VF_i}$ is the speed command obtained through the path following vector field for UAV No.i;
$v^c_{VF_{i+1}}$ is the speed command obtained through the path following vector field for UAV No.$(i+1)$.

It is also possible to implement a simplified version of Sub-algorithm (5) in the form:

$$\begin{aligned} v^c_i &= \begin{cases} v_{\max}, & \text{if} \quad \text{Condition 1;} \\ v^c_{VF_i}, & \text{if} \quad \text{Condition 2,} \end{cases} \\ v^c_{i+1} &= \begin{cases} v_{\min}, & \text{if} \quad \text{Condition 1;} \\ v^c_{VF_{i+1}}, & \text{if} \quad \text{Condition 2.} \end{cases} \end{aligned} \tag{6}$$

In this case, the artificial potential field is used only for course control.

The choice of values $v_{\max}$ and $v_{\min}$ should be made taking into account the dynamics of the UAV, since a significant decrease in speed also causes a strong loss of flight altitude. The operation of Sub-algorithm (6) implies the acceleration of the overtaking maneuver by increasing the speed of the overtaking UAV and reducing the speed of the overtaken UAV by higher values than it is provided by the path following vector field algorithm. These conditions (5)-(6) themselves imply that the velocity components in Sub-algorithms 2 and 4 are multiplied by the same positive coefficient if the velocity modulus is outside the limit values. Therefore, for clarity of presentation, this multiplication by a coefficient is not written out in the stability analysis below. This can be done since there is no influence on the process of the corresponding reasoning.

Together, Sub-algorithms 1-4, (5)-(6) constitute an overall Algorithm for collision avoidance between UAVs in the circular formation motion problem, which we denoted earlier as APFfCM.

Consider a system of two fixed-wing UAVs numbered i and $i+1$ that need to perform collision avoidance. For such a system, the following theorem is satisfied when using the proposed algorithm. A proof of stability in the case of applying an artificial potential field in the object tracking problem was given, for example, in [27]. However, the algorithm in that paper is fundamentally different from the one we consider, so the proof itself is also disparate.

The considered system of two fixed-wing UAV No.i and No.$(i+1)$, taking into account (1) can be represented in a generalized form:

$$\dot{d}\left(\mathbf{q}_i, \mathbf{q}_{i+1}\right) = \left(\nabla_{\mathbf{q}_i - \mathbf{q}_{i+1}} d\left(\mathbf{q}_i, \mathbf{q}_{i+1}\right)\right)^{\mathrm{T}} \left(\dot{\mathbf{q}}_i - \dot{\mathbf{q}}_{i+1}\right), \tag{7}$$

$$\begin{aligned}\dot{\hat{\mathbf{d}}} &= \left(\dot{\hat{d}}_k\right)_{k=\overline{i,\,i+1}} \\ &\triangleq \left(\begin{bmatrix} \dot{p}_i^n & \dot{p}_i^e \end{bmatrix}\begin{bmatrix} \cos\varphi_i & \sin\varphi_i \end{bmatrix}^{\mathrm{T}}\right)\otimes\begin{bmatrix} 1 \\ 0 \end{bmatrix} \\ &\quad + \left(\begin{bmatrix} \dot{p}_{i+1}^n & \dot{p}_{i+1}^e \end{bmatrix}\begin{bmatrix} \cos\varphi_{i+1} & \sin\varphi_{i+1} \end{bmatrix}^{\mathrm{T}}\right)\otimes\begin{bmatrix} 0 \\ 1 \end{bmatrix}.\end{aligned} \tag{8}$$

The following notation is used here:

$\varphi_{k\in\{i,\,i+1\}}$ is the phase angle of rotation for the k-th UAV;
$d_{k\in\{i,\,i+1\}}$ is the distance to the center of rotation for the k-th UAV;
ρ is the radius of the rotation orbit for the formation;
block vector $\hat{\mathbf{d}} \in \mathbb{R}^{2\times 1}$ is defined as

$$\hat{\mathbf{d}} = \left(\hat{d}_k\right)_{k=\overline{i,\,i+1}} \triangleq \left(\|\mathbf{q}_i - \mathbf{c}\|_2 - \rho\right)\otimes\begin{bmatrix} 1 \\ 0 \end{bmatrix} + \left(\|\mathbf{q}_{i+1} - \mathbf{c}\|_2 - \rho\right)\otimes\begin{bmatrix} 0 \\ 1 \end{bmatrix}$$

through the $\mathbf{c} \in \mathbb{R}^{2\times 1}$ as the position vector of the rotation center for the UAV formation. That is, the elements of the vector $\hat{\mathbf{d}}$ are the distances to the circular path given by the distances $d_{k\in\{i,\,i+1\}}$ from the considered UAV to the rotation center of the formation:

$$\hat{d}_{k\in\{i,\,i+1\}} \triangleq d_{k\in\{i,\,i+1\}} - \rho.$$

The equilibrium position $d(\mathbf{q}_i, \mathbf{q}_{i+1}) = d_o$ is considered for the nominal system (6), i.e., in the case when the control algorithm fulfills the condition $\eta_i = \eta_{i+1} = 0$. Then the summands $\eta_i \sin\chi_i^c$, $\eta_i \cos\chi_i^c$, $\eta_{i+1}\sin\chi_{i+1}^c$, $\eta_{i+1}\cos\chi_{i+1}^c$ act as non-vanishing perturbations.

Let us introduce the domains $\mathscr{D}_1$ and $\mathscr{D}_2$:

$$\mathscr{D}_1 \triangleq \{d(\mathbf{q}_i, \mathbf{q}_{i+1}) \in \mathbb{R} \mid d(\mathbf{q}_i, \mathbf{q}_{i+1}) \leqslant d_o \wedge d(\mathbf{q}_i, \mathbf{q}_{i+1}) \neq 0\},$$

$$\mathscr{D}_2 \triangleq \{d(\mathbf{q}_i, \mathbf{q}_{i+1}) \in \mathbb{R} \mid d(\mathbf{q}_i, \mathbf{q}_{i+1}) > d_o\}.$$

We consider the behavior of the system (8) only in the domain $\mathscr{D}_2$, since we are interested in the convergence of the drones to a circular orbit of rotation only after they have performed an evasive maneuver and left the "danger zone".

Theorem, 1. Consider domain $\mathscr{D}_1 \cup \mathscr{D}_2$. Under the action of the APFfCM algorithm, the trajectories of system (7) are uniformly bounded (UB), and the equilibrium position of system (8) is locally asymptotically stable in the domain $\mathscr{D}_2$. In addition, there is no collision event between UAV No.i and UAV No.$(i+1)$.

Proof. As noted earlier, the final APFfCM control algorithm uses a rotationally modified artificial potential function for UAV No.i and a FIRAS artificial potential function for UAV No.$(i+1)$. For the distances to the center of rotation $\|\mathbf{d}_i\|_2$ and $\|\mathbf{d}_{i+1}\|_2$, the condition that $\|\mathbf{d}_i\|_2 \neq 0 \wedge \|\mathbf{d}_{i+1}\|_2 \neq 0$ is assumed since the calculation method of some parameters is not defined when this condition is violated.

Let us introduce the following function $\mathbb{V}$ as a candidate Lyapunov function using (2):

$$\mathbb{V} = \begin{cases} \frac{1}{2}\kappa \left\{ \begin{array}{l} U_r^{\text{APFfCM}}(\mathbf{q}_i, \mathbf{q}_{i+1}) + \\ + U_r^{\text{APFfCM}}(\mathbf{q}_{i+1}, \mathbf{q}_i) \end{array} \right\}, & \text{if} \quad d(\mathbf{q}_i, \mathbf{q}_{i+1}) \leqslant d_o; \\ \\ \frac{1}{2}\hat{\mathbf{d}}^{\mathrm{T}}\hat{\mathbf{d}}, & \text{if} \quad d(\mathbf{q}_i, \mathbf{q}_{i+1}) > d_o, \end{cases} \tag{9}$$

where constant coefficient $\kappa \in \mathbb{R}_{>0}$.

The derivative of the candidate Lyapunov function $\mathbb{V}$ (9) can be represented in this form:

$$\dot{\mathbb{V}} = \begin{cases} \frac{1}{2}\kappa \left\{ \begin{array}{l} \dot{U}_r^{\text{APFfCM}}(\mathbf{q}_i, \mathbf{q}_{i+1}) + \\ + \dot{U}_r^{\text{APFfCM}}(\mathbf{q}_{i+1}, \mathbf{q}_i) \end{array} \right\}, & \text{if} \quad d(\mathbf{q}_i, \mathbf{q}_{i+1}) \leqslant d_o; \\ \\ \hat{\mathbf{d}}^{\mathrm{T}}\dot{\hat{\mathbf{d}}}, & \text{if} \quad d(\mathbf{q}_i, \mathbf{q}_{i+1}) > d_o. \end{cases} \tag{10}$$

Consider the case of $d(\mathbf{q}_i, \mathbf{q}_{i+1}) \leqslant d_o$. We can obtain the following representation for the derivative $\dot{U}_r^{\text{APFfCM}}(\mathbf{q}_i, \mathbf{q}_{i+1})$:

$$\dot{U}_r^{\text{APFfCM}}(\mathbf{q}_i, \mathbf{q}_{i+1}) = \left(\nabla_{\mathbf{p}_{i,i+1}} U_r^{\text{APFfCM}}\right)^{\mathrm{T}} \dot{\mathbf{p}}_{i,i+1},$$

where $\mathbf{p}_{i,i+1} \stackrel{\Delta}{=} \mathbf{q}_i - \mathbf{q}_{i+1}$. Similarly

$$\dot{U}_r^{\text{APFfCM}}(\mathbf{q}_{i+1}, \mathbf{q}_i) = \left(\nabla_{\mathbf{p}_{i+1,i}} U_r^{\text{APFfCM}}\right)^{\text{T}} \dot{\mathbf{p}}_{i+1,i}.$$

Note that the following relation holds:

$$\begin{aligned}\nabla_{\mathbf{p}_{i,i+1}} U_r^{\text{APFfCM}}(\mathbf{q}_i, \mathbf{q}_{i+1}) &= \nabla_{\mathbf{q}_i} U_r^{\text{APFfCM}}(\mathbf{q}_i, \mathbf{q}_{i+1}) \\ &= -\nabla_{\mathbf{q}_{i+1}} U_r^{\text{APFfCM}}(\mathbf{q}_i, \mathbf{q}_{i+1}) \\ &= -\nabla_{\mathbf{q}_{i+1}} U_r^{\text{APFfCM}}(\mathbf{q}_{i+1}, \mathbf{q}_i).\end{aligned}$$

Taking into account the above, we can obtain

$$\begin{aligned}\dot{U}_r^{\text{APFfCM}}(\mathbf{q}_i, \mathbf{q}_{i+1}) + \\ +\dot{U}_r^{\text{APFfCM}}(\mathbf{q}_{i+1}, \mathbf{q}_i)\end{aligned} &= \left\{ \begin{array}{l} \left(\nabla_{\mathbf{p}_{i,i+1}} U_r^{\text{APFfCM}}(\mathbf{q}_i, \mathbf{q}_{i+1})\right)^{\text{T}} \dot{\mathbf{p}}_{i,i+1} + \\ +\left(\nabla_{\mathbf{p}_{i+1,i}} U_r^{\text{APFfCM}}(\mathbf{q}_{i+1}, \mathbf{q}_i)\right)^{\text{T}} \dot{\mathbf{p}}_{i+1,i} \end{array} \right\} \\ &= \left\{ \begin{array}{l} \left(\nabla_{\mathbf{q}_i} U_r^{\text{APFfCM}}(\mathbf{q}_i, \mathbf{q}_{i+1})\right)^{\text{T}} (\dot{\mathbf{q}}_i - \dot{\mathbf{q}}_{i+1}) + \\ +\left(\nabla_{\mathbf{q}_{i+1}} U_r^{\text{APFfCM}}(\mathbf{q}_{i+1}, \mathbf{q}_i)\right)^{\text{T}} (\dot{\mathbf{q}}_{i+!} - \dot{\mathbf{q}}_i) \end{array} \right\} \\ &= \left(\nabla_{\mathbf{q}_i} \left\{ \begin{array}{l} U_r^{\text{APFfCM}}(\mathbf{q}_i, \mathbf{q}_{i+1}) + \\ +U_r^{\text{APFfCM}}(\mathbf{q}_{i+1}, \mathbf{q}_i) \end{array} \right\}\right)^{\text{T}} \dot{\mathbf{q}}_i + \\ &\quad + \left(\nabla_{\mathbf{q}_{i+1}} \left\{ \begin{array}{l} U_r^{\text{APFfCM}}(\mathbf{q}_i, \mathbf{q}_{i+1}) + \\ +U_r^{\text{APFfCM}}(\mathbf{q}_{i+1}, \mathbf{q}_i) \end{array} \right\}\right)^{\text{T}} \dot{\mathbf{q}}_{i+1} \\ &= 2\left(\nabla_{\mathbf{q}_i} U_r^{\text{APFfCM}}(\mathbf{q}_i, \mathbf{q}_{i+1})\right)^{\text{T}} \dot{\mathbf{q}}_i + \\ &\quad + 2\left(\nabla_{\mathbf{q}_{i+1}} U_r^{\text{APFfCM}}(\mathbf{q}_{i+1}, \mathbf{q}_i)\right)^{\text{T}} \dot{\mathbf{q}}_{i+1}.\end{aligned}$$

Given the APFfCM algorithm, the derivative of the candidate Lyapunov function (10) takes the form:

$$\frac{1}{2}\kappa\left\{\begin{array}{l}\dot{U}_r^{\mathrm{APFfCM}}(\mathbf{q}_i,\mathbf{q}_{i+1})+\\ +\dot{U}_r^{\mathrm{APFfCM}}(\mathbf{q}_{i+1},\mathbf{q}_i)\end{array}\right\}=$$

$$=\frac{1}{2}\kappa\left\{\begin{array}{c}2\left(\nabla_{\mathbf{q}_i}U_r^{\mathrm{APFfCM}}(\mathbf{q}_i,\mathbf{q}_{i+1})\right)^{\mathrm{T}}\dot{\mathbf{q}}_i+\\ +2\left(\nabla_{\mathbf{q}_{i+1}}U_r^{\mathrm{APFfCM}}(\mathbf{q}_{i+1},\mathbf{q}_i)\right)^{\mathrm{T}}\dot{\mathbf{q}}_{i+1}\end{array}\right\}=$$

$$=\kappa\left\{\begin{array}{c}\left(\nabla_{\mathbf{q}_i}U_r^{\mathrm{APFfCM}}(\mathbf{q}_i,\mathbf{q}_{i+1})\right)^{\mathrm{T}}\times\\ \times\left[-\nabla_{\mathbf{q}_i}U_r^{\mathrm{APFfCM}}(\mathbf{q}_i,\mathbf{q}_{i+1})\,\mathbf{R}(\lambda)+\eta_i\mathbf{f}^{VF}(\mathbf{q}_i)\right]+\\ +\left(\nabla_{\mathbf{q}_{i+1}}U_r^{\mathrm{APFfCM}}(\mathbf{q}_{i+1},\mathbf{q}_i)\right)^{\mathrm{T}}\times\\ \times\left[-\nabla_{\mathbf{q}_{i+1}}U_r^{\mathrm{APFfCM}}(\mathbf{q}_{i+1},\mathbf{q}_i)+\eta_{i+1}\mathbf{f}^{VF}(\mathbf{q}_{i+1})\right]\end{array}\right\}.$$

This equation is transformed to the following form:

$$\frac{1}{2}\kappa\left\{\begin{array}{l}\dot{U}_r^{\mathrm{APFfCM}}(\mathbf{q}_i,\mathbf{q}_{i+1})+\\ +\dot{U}_r^{\mathrm{APFfCM}}(\mathbf{q}_{i+1},\mathbf{q}_i)\end{array}\right\}=$$

$$=\kappa\left\{\begin{array}{l}-\mathrm{K}\left[\left(p_i^n-p_{i+1}^n\right)\eta_i\cos\chi_i^c+\left(p_i^e-p_{i+1}^e\right)\eta_i\sin\chi_i^c\right]-\\ -\mathrm{K}\left[\left(p_{i+1}^n-p_i^n\right)\eta_{i+1}\cos\chi_{i+1}^c+\left(p_{i+1}^e-p_i^e\right)\eta_{i+1}\sin\chi_{i+1}^c\right]\\ \underbrace{+\mathrm{K}^2\left(p_i^n-p_{i+1}^n\right)\left(p_i^e-p_{i+1}^e\right)-\mathrm{K}^2\left(p_i^n-p_{i+1}^n\right)\left(p_i^e-p_{i+1}^e\right)}_{=0}-\\ -\mathrm{K}^2\left[\left(p_i^n-p_{i+1}^n\right)^2+\left(p_i^e-p_{i+1}^e\right)^2\right]\end{array}\right\}\quad(11)$$

$$=\kappa\left\{\begin{array}{l}-\mathrm{K}\left[\begin{array}{l}\left(p_i^n-p_{i+1}^n\right)\left(\eta_i\cos\chi_i^c-\eta_{i+1}\cos\chi_{i+1}^c\right)\\ +\left(p_i^e-p_{i+1}^e\right)\left(\eta_i\sin\chi_i^c-\eta_{i+1}\sin\chi_{i+1}^c\right)\end{array}\right]-\\ -\mathrm{K}^2\left[\left(p_i^n-p_{i+1}^n\right)^2+\left(p_i^e-p_{i+1}^e\right)^2\right]\end{array}\right\}.$$

Here $\mathrm{K}\triangleq k_{r_i}\left(\frac{1}{d(\mathbf{q}_i,\mathbf{q}_{i+1})}-\frac{1}{d_o}\right)\frac{1}{d^3(\mathbf{q}_i,\mathbf{q}_{i+1})}\geqslant 0$.

Let us introduce the notation:

$$x\triangleq p_i^e-p_{i+1}^e,\quad y\triangleq p_i^n-p_{i+1}^n,$$
$$\delta_x\triangleq\eta_i\sin\chi_i^c-\eta_{i+1}\sin\chi_{i+1}^c,\quad \delta_y\triangleq\eta_i\cos\chi_i^c-\eta_{i+1}\cos\chi_{i+1}^c.$$

Then we represent the obtained expression (11) in the form

$$\Gamma \triangleq \underbrace{\kappa \mathrm{K}^2 \left(-x^2 - y^2\right)}_{\prec 0} + \kappa \mathrm{K} \left(-\delta_x x - \delta_y y\right), \tag{12}$$

where $\delta_x \in \mathbb{R}$ and $\delta_y \in \mathbb{R}$ are values that should turn out to be sufficiently small, as will be explained later. It is possible to make them so by choosing small parameters η_i and η_{i+1}. The second summand in expression (12) is indefinite. Note that the condition $d\left(\mathbf{q}_i, \mathbf{q}_{i+1}\right) \triangleq \left\|\mathbf{q}_i - \mathbf{q}_{i+1}\right\|_2 \to 0$ corresponds to the divergence of the system trajectories from the equilibrium position. At the same time, the condition $d\left(\mathbf{q}_i, \mathbf{q}_{i+1}\right) \triangleq \left\|\mathbf{q}_i - \mathbf{q}_{i+1}\right\|_2 \to d_o$ corresponds, on the contrary, to the convergence of the trajectories to the equilibrium position. In the case $d\left(\mathbf{q}_i, \mathbf{q}_{i+1}\right) \to 0$, the quadratic summand $\kappa \mathrm{K}^2 \left(-x^2 - y^2\right)$ in (12) will dominate the linear summand $\kappa \mathrm{K} \left(-\delta_x x - \delta_y y\right)$ if it takes positive values. If it takes negative values, then the condition we need is satisfied. Thus, Γ (12) is negative semidefinite except for some regions near the equilibrium position. However, this region can be made as small as desired by the choice of parameters δ_x and δ_y small enough. The trajectories of the system entering this region will not be able to leave it, so uniform boundedness (UB) of trajectories is observed. Note that such a consideration was used in many works, for example, in [28].

To clearly illustrate the above reasoning, we made a graphical representation of the functions. Figure 3(a) shows the three-dimensional view in the case when the summand $\kappa \mathrm{K} \left(-\delta_x x - \delta_y y\right)$ is excluded from the function Γ (12), i.e., the function $\Gamma^{\mathrm{def}} \triangleq \underbrace{\kappa \mathrm{K}^2 \left(-x^2 - y^2\right)}_{\prec 0}$ is considered. Figure 3(b) shows the case where the summand $\kappa \mathrm{K} \left(-\delta_x x - \delta_y y\right)$ is present, that is, the function Γ (12) itself is plotted. The parameters chosen were: $d_o = 3, \quad \delta_x = \delta_y = 0.25, \quad \kappa = 1$. As can be seen, Γ^{def} is always negative or equal to zero, but Γ has, near the equilibrium position, some elevation entering the positive region of values. For an additional illustration, Figure 4 is presented, showing in blue the region near the equilibrium position where the derivative of the Lyapunov function candidate takes positive values. The white color in this case shows the region where conversely the derivative takes negative values. Here the parameters chosen were: $d_o = 3, \quad \delta_x = \delta_y = 0.0015, \quad \kappa = 1$.

Obviously, if the above result holds for the entire region $\mathscr{D}_1$, then it also holds when the additional condition $T_{prod} < T_{tresh}$ is imposed.

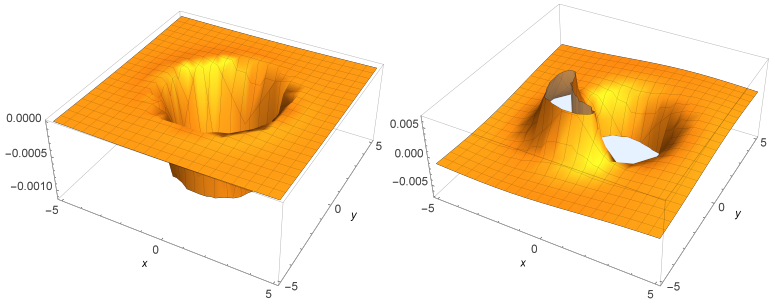

a) function Γ^{def} b) function Γ

Fig. 3. Graphical plotting of the candidate Lyapunov function derivative

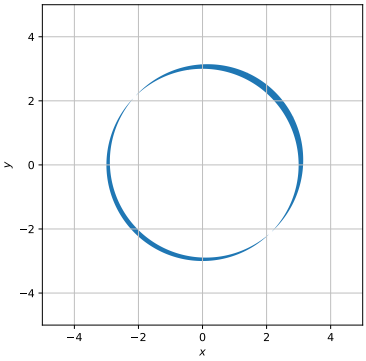

Fig. 4. Unstable region near the equilibrium position

If $d(\mathbf{q}_i, \mathbf{q}_{i+1}) > d_o$, then, given the circular formation control algorithm [25, 26], the derivative of the candidate Lyapunov function (10) takes the form:

$$\begin{aligned}\hat{\mathbf{d}}^T\dot{\hat{\mathbf{d}}} &= \hat{d}_{k\in\{i,i+1\}}\left(\dot{p}^n_{k\in\{i,i+1\}}\cos\varphi_{k\in\{i,i+1\}}\right)+\\ &+\hat{d}_{k\in\{i,i+1\}}\left(\dot{p}^e_{k\in\{i,i+1\}}\sin\varphi_{k\in\{i,i+1\}}\right)\\ &= k^{vf}_{k\in\{i,i+1\}}\hat{d}_{k\in\{i,i+1\}}\cos\varphi_{k\in\{i,i+1\}}\cos\chi^c_{k\in\{i,i+1\}}+\\ &+k^{vf}_{k\in\{i,i+1\}}\hat{d}_{k\in\{i,i+1\}}\sin\varphi_{k\in\{i,i+1\}}\sin\chi^c_{k\in\{i,i+1\}}\\ &= k^{vf}_{k\in\{i,i+1\}}\hat{d}_{k\in\{i,i+1\}}\cos\left(\chi^c_{k\in\{i,i+1\}}-\varphi_{k\in\{i,i+1\}}\right).\end{aligned}$$

Here $\hat{d}_{k\in\{i,i+1\}}$ is the deviation of the distance to the rotation center of the formation, defined earlier in (8); $\varphi_{k\in\{i,\,i+1\}}$ is the angle also defined earlier in (8); $\chi^c_{k\in\{i,i+1\}}$ is the course control command given according to the algorithm for circular path following [25, 26]; $k^{vf}_{\max} > k^{vf}_{k\in\{i,i+1\}} > k^{vf}_{\min} > 0$ is the parameter that is determined by the condition on the UAV's speed in the same control algorithm for circular path following. In view of the way the value $\chi^c_{k\in\{i,i+1\}}$ is calculated in this control algorithm for circular path following [25, 26], we can obtain:

$$\begin{aligned}\hat{\mathbf{d}}^{\mathrm{T}}\dot{\hat{\mathbf{d}}} &= -k^{vf}_{k\in\{i,i+1\}}\hat{d}_{k\in\{i,i+1\}}\sin\left(\arctan\left(k_o\hat{d}_{k\in\{i,i+1\}}\right)\right)\\ &= -\hat{d}^2_{k\in\{i,i+1\}}k^{vf}_{k\in\{i,i+1\}}k_o\left(1+\left(k_o\hat{d}_{k\in\{i,i+1\}}\right)^2\right)^{-1/2},\end{aligned}$$

where $k_o \in \mathbb{R}_{>0}$ is a tunable parameter. Note that in this case the function $\hat{\mathbf{d}}^{\mathrm{T}}\dot{\hat{\mathbf{d}}}$ turns out to be negative definite along the trajectories of the system. Given the positive definiteness of function $\mathbb{V}$ (9), this means the convergence of drones to a circular orbit of rotation.

Note that for the sake of brevity, the case $d(\mathbf{q}_i,\mathbf{q}_{i+1}) \leqslant d_o \wedge T_{prod} \geqslant T_{tresh}$ is not considered separately, since the stability considerations are similar to those given for the case $d(\mathbf{q}_i,\mathbf{q}_{i+1}) > d_o$. At the same time, we assume that the danger of a collision when $T_{prod} \geqslant T_{tresh}$ vanishes due to the occurrence of the overtaking event.

In summary, the derivative of the candidate Lyapunov function (10) along the trajectories of system (7)-(8), in the case of the proposed APFfCM algorithm and the circular path following algorithm [25, 26], takes the form:

$$\dot{\mathbb{V}} = \begin{cases} \kappa\left\{\begin{array}{l} -\mathrm{K}\left[\begin{array}{l}\left(p^n_i-p^n_{i+1}\right)\left(\eta_i\cos\chi^c_i-\eta_{i+1}\cos\chi^c_{i+1}\right)\\ +\left(p^e_i-p^e_{i+1}\right)\left(\eta_i\sin\chi^c_i-\eta_{i+1}\sin\chi^c_{i+1}\right)\end{array}\right]\\ -\mathrm{K}^2\left[\left(p^n_i-p^n_{i+1}\right)^2+\left(p^e_i-p^e_{i+1}\right)^2\right]\end{array}\right\},\\ \qquad\qquad\qquad\qquad\qquad\qquad \text{if } d(\mathbf{q}_i,\mathbf{q}_{i+1}) \leqslant d_o;\\ -\hat{d}^2_{k\in\{i,i+1\}}\times\\ \times k^{vf}_{k\in\{i,i+1\}}k_o\left(1+\left(k_o\hat{d}_{k\in\{i,i+1\}}\right)^2\right)^{-1/2}, \quad \text{if } d(\mathbf{q}_i,\mathbf{q}_{i+1}) > d_o.\end{cases}$$

Hence, we conclude that the derivative of the candidate Lyapunov function along the trajectories of the system (8) is negative definite in the

domain $\mathscr{D}_2$. From this, taking into account the positive definiteness of the function (9), the local asymptotic stability is obtained.

Since uniform boundedness (UB) (so-called Lagrange stability) is satisfied for all trajectories of the system (7), the candidate Lyapunov function itself is bounded for bounded states. The event of a collision between UAVs No.i and No.$(i+1)$ will take the candidate Lyapunov function (9) to $+\infty$. Thus, we can be sure that such a collision will not occur. As a result, by using the direct Lyapunov method, it is possible to guarantee the absence of a collision event. This completes the proof.

3. Simulations on full nonlinear fixed-wing drone models. Further, we present the results of modeling the algorithm in MATLAB/Simulink on full nonlinear models of four small "flying wing" type Zagi UAVs equipped with tuned autopilots. These models are built according to the monograph [29]. In the same monograph, the model parameters and features of its implementation in MATLAB/Simulink environment, as well as the details of autopilot synthesis are described.

Figure 5 shows the UAV flight trajectories in the case of using the APFfCM algorithm proposed in this study.

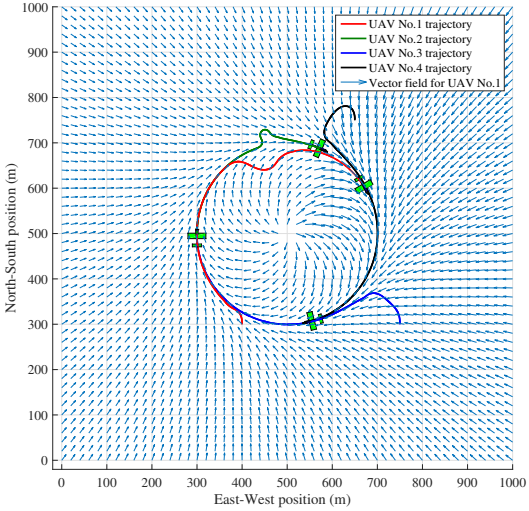

Fig. 5. UAV flight trajectories in case of using APFfCM algorithm

The radius of the "danger zone" ("safety radius") was chosen to be $d_o = 100$ m. We also selected $T_{tresh} = 5 \cdot 10^3$. In the specified figure, the

deviations of the trajectories as a result of performing an evasive maneuver by both UAV No.i and UAV No.$(i+1)$ (in this case, UAV No.1 and UAV No.2) are clearly visible.

Figure 6 shows the distance between UAV No.i and UAV No.$(i+1)$ during the simulation. In this graph, the peak occurring at about 32 seconds is due to the fact that starting at about 32 seconds, the UAVs commence to move closer together on converging courses. This in turn is caused by the fact that after moving away to a reasonably safe distance by about 32 seconds, the UAVs begin to return to collective circular motion, which assumes converging courses while moving.

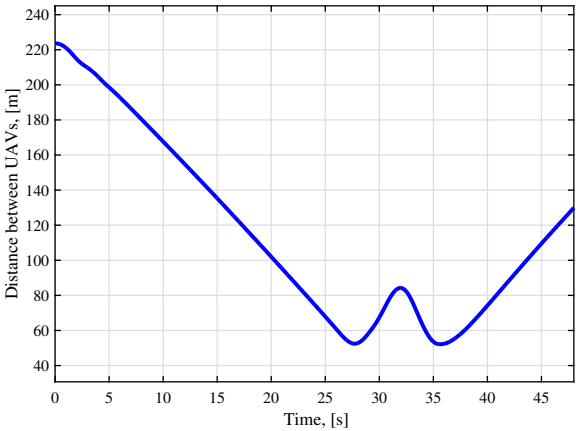

Fig. 6. Distance between UAVs during a flight in case of using APFfCM algorithm

It can also be observed in Figure 6 that the evasive maneuver does not start immediately after exceeding the “safety radius”. This is due to the fact that the path following vector field, rather than the artificial potential field, has a stronger influence at first. As a result, there is a balance between the necessities of maintaining the overall circular strategy and collision avoidance. Figure 7 shows how the value of the triple product T_{prod} changed. In this graph, the moment of sign change corresponds to the moment one UAV overtakes another UAV. From the comparison of Figures 1 and 5, the advantage of the approach proposed in this paper over the algorithm from [20] is clearly visible: UAVs do not make unnecessary meaningless turnarounds and save resources. This advantage arises mainly because the algorithm from [20] was designed for rotary-wing drones and therefore is not directly applicable to fixed-wing UAVs.

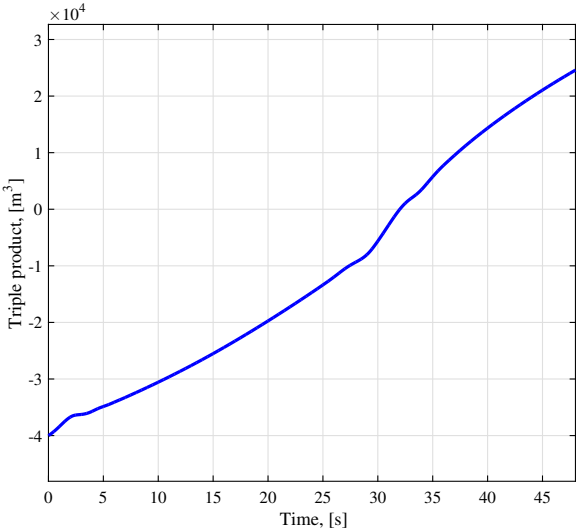

Fig. 7. Changes in the value of the triple product T_{prod}

To numerically compare the proposed algorithm with the standard algorithm, the following metrics are considered. Integral course angle I^{course}:

$$I^{\text{course}} \triangleq \int_{t_0}^{T} \left(\left| \chi^i \right| + \left| \chi^{i+1} \right| \right) dt,$$

where t_0 is the start time of the collision avoidance maneuver; T is the end time of this maneuver; χ^i is the course angle of the UAV No.i; χ^{i+1} is the course angle of the UAV No.$(i+1)$.

Integral path error I^{path}:

$$I^{\text{path}} \triangleq \int_{t_0}^{T} \left(\left| e^i \right| + \left| e^{i+1} \right| \right) dt,$$

where e^i is the path error of the UAV No.i; $e^i + 1$ is the path error of the UAV No.$(i+1)$.

Integral control effort U:

$$U \triangleq \frac{1}{\alpha\chi} \int_{t_0}^{T} \left\{ \left| \chi_c^i - \chi^i \right| + \left| \chi_c^{i+1} - \chi^{i+1} \right| \right\} dt,$$

where α^{χ} is the coefficient determined by the course angle control loop; χ_c^i is the commanded course angle of the UAV No.i; χ_c^{i+1} is the commanded course angle of the UAV No.$(i+1)$.

The maximum total angle of deviation from the initial course χ^{sum}:

$$\chi^{\text{sum}} \triangleq \max_{\chi^i \in \mathbb{R}_{>0}} \chi^i + \max_{\chi^i \in \mathbb{R}_{<0}} \left|\chi^i\right| + \max_{\chi^{i+1} \in \mathbb{R}_{>0}} \chi^{i+1} + \max_{\chi^{i+1} \in \mathbb{R}_{<0}} \left|\chi^{i+1}\right|.$$

Table 1 shows the numerical values obtained from the simulation to compare the APFfCM and standard APF algorithms.

Table 1. Algorithm comparison results

Algorithm variant	I^{course}, rad	I^{path}, m	U, rad/s	χ^{sum}, rad
APFfCM	62.38	798.1	43.76	4.69
Standard APF	107.42	966.1	43.31	7.76

From the comparison of the algorithms, we can conclude that the control effort is almost the same. At the same time, the integral course angle and the maximum total angle of deviation from the original course are significantly larger for the standard APF algorithm. This result is explained by the fact that in the standard APF algorithm, a complete turn of one of the UAVs occurs, which also affects the final trajectory of the other UAV involved in collision avoidance. The integral path error is much larger for the standard APF, which affects the time to return to the final circular path line and the subsequent construction of the given formation geometry by the drones.

4. Conclusion. In this study, a collision avoidance algorithm is proposed for coordinated circular motion of a group of autonomous fixed-wing type UAVs (drones). In this case, one of the drones must overtake the other in order to build a given formation geometry. At the same time, the formation must keep following a circular path line. Compared to the algorithm for rotary-wing UAVs, a modification was required to account for the limited maneuverability of fixed-wing drones due to their nonholonomic dynamics. Also, the uniform boundedness (UB) of the system trajectories allowed to guarantee that collision events between UAVs will not occur. The simulation results on the full nonlinear models of the fixed-wing type UAVs clearly show the advantages of the proposed approach.

References

1. Platonov A.K., Kiril'chenko A.A., Kolganov M.A. [The Potential Field Approach in the Path Finding Problem: History and Perspectives]. Preprinty Instituta im. M.V. Keldysha RAN – Keldysh Institute preprints. 2001. KIAM Preprint № 40. (In Russ.).
2. Khatib O. Real-Time Obstacle Avoidance for Manipulators and Mobile Robots. The international journal of robotics research. 1986. vol. 5. no. 1. pp. 90–98.

3. Bojian L., Jun F., Yunxiao Q., Aijun L. Precise Formation Control for the Multi-agent Systems Based on Tilted Potential Field with Collision Avoidance. International Conference on Guidance, Navigation and Control. Lecture Notes in Electrical Engineering. 2023. vol. 845. pp. 84–93. DOI: 10.1007/978-981-19-6613-2 _10.
4. Alhaddad M., Mironov K., Staroverov A., Panov A. Neural Potential Field for Obstacle-Aware Local Motion Planning. 2023. arxiv preprint arXiv:2310.16362. DOI: 10.48550/arXiv.2310.16362.
5. Filimonov A.B., Filimonov N.B. The Concept of Fairway in Problems of Potential Guidance of Mobile Robots. Optoelectronics, Instrumentation and Data Processing. 2022. vol. 58. no. 4. pp. 366–372. DOI: 10.3103/S8756699022040057.
6. Szczepanski R., Tarczewski T., Erwinski K. Energy Efficient Local Path Planning Algorithm Based on Predictive Artificial Potential Field. IEEE Access. 2022. vol. 10. pp. 39729–39742. DOI: 10.1109/ACCESS.2022.3166632.
7. Mikishanina E.A., Platonov P.S. [Control of a Wheeled Robot on a Plane with Obstacles]. Mekhatronika, Avtomatizatsiya, Upravlenie – Mechatronics, Automation, Control. 2024. vol. 25. no. 2. pp. 93–100. (In Russ.).
8. Xi Z., Han H., Cheng J., Lv M. Reducing Oscillations for Obstacle Avoidance in a Dense Environment Using Deep Reinforcement Learning and Time-Derivative of an Artificial Potential Field. Drones. 2024. vol. 8. no. 3. DOI: 10.3390/drones8030085.
9. De Medio C., Nicolò F., Oriolo G. Robot Motion Planning Using Vortex Fields. New Trends in Systems Theory. Progress in Systems and Control Theory. Boston: Birkhäuser Boston. 1991. vol. 7. pp. 237–244.
10. De Medio C., Oriolo G. Robot Obstacle Avoidance Using Vortex Fields. Advances in Robot Kinematics. Vienna: Springer Vienna. 1991. pp. 227–235. DOI: 10.1007/978-3-7091-4433-6 _26.
11. De Luca A., Oriolo G. Local incremental planning for nonholonomic mobile robots. Proc. IEEE Int. Conf. Robot. Autom. 1994. pp. 104–110. DOI: 10.1109/ROBOT.1994.351003.
12. Martis W.P., Rao S. Cooperative Collision Avoidance in Mobile Robots using Dynamic Vortex Potential Fields. 9th Int. Conf. Autom. Robot. Appl. (ICARA 2023). 2023. pp. 60–64. DOI: 10.1109/ICARA56516.2023.10125851.
13. Choi D., Lee K., Kim D. Enhanced Potential Field-Based Collision Avoidance for Unmanned Aerial Vehicles in a Dynamic Environment. AIAA Scitech 2020 Forum. 2020. DOI: 10.2514/6.2020-0487.
14. Choi D., Kim D., Lee K. Enhanced Potential Field-Based Collision Avoidance in Cluttered Three-Dimensional Urban Environments. Appl. Sci. 2021. vol. 11. no. 22. DOI: 10.3390/app112211003.
15. Choi D., Chhabra A., Kim D. Intelligent cooperative collision avoidance via fuzzy potential fields. Robotica. 2022. vol. 40. no. 6. pp. 1919–1938. DOI: 10.1017/S0263574721001454.
16. Batinovic A., Goricanec J., Markovic L., Bogdan S. Path Planning with Potential Field-Based Obstacle Avoidance in a 3D Environment by an Unmanned Aerial Vehicle. International Conference on Unmanned Aircraft Systems (ICUAS). 2022. pp. 394–401. DOI: 10.1109/ICUAS54217.2022.9836159.
17. Goricanec J., Milas A., Markovic L., Bogdan S. Collision-Free Trajectory Following With Augmented Artificial Potential Field Using UAVs. IEEE Access. 2023. vol. 11. pp. 83492–83506. DOI: 10.1109/ACCESS.2023.3303109.
18. Szczepanski R. Safe Artificial Potential Field – Novel Local Path Planning Algorithm Maintaining Safe Distance From Obstacles. IEEE Robot. Autom. Lett. 2023. vol. 8. no. 8. pp. 4823–4830. DOI: 10.1109/LRA.2023.3290819.

19. Su Y.-H., Bhowmick P., Lanzon A. A Fixed-time Formation-containment Control Scheme for Multi-agent Systems with Motion Planning: Applications to Quadcopter UAVs. IEEE Transactions on Vehicular Technology. 2024. vol. 73. no. 7. pp. 9495–9507. DOI: 10.1109/TVT.2024.3382489.
20. Muslimov T. Curl-Free Vector Field for Collision Avoidance in a Swarm of Autonomous Drones. Lecture Notes in Computer Science. Interactive Collaborative Robotics (ICR 2023). 2023. vol. 14214. pp. 369–379.
21. Muslimov T., Kozlov E., Munasypov R. Drone Swarm Movement without Collisions with Fixed Obstacles Using a Hybrid Algorithm Based on Potential Functions. International Russian Automation Conference (RusAutoCon). 2023. pp. 781–785.
22. Gao Y., Bai C., Fu R., Quan Q. A non-potential orthogonal vector field method for more efficient robot navigation and control. Rob. Auton. Syst. 2023. vol. 159. DOI: 10.1016/j.robot.2022.104291.
23. Park C., Cho N., Lee K., Kim Y. Formation Flight of Multiple UAVs via Onboard Sensor Information Sharing. Sensors. 2015. vol. 15. no. 7. pp. 17397–17419.
24. Kim S., Cho H., Jung D. Circular Formation Guidance of Fixed-Wing UAVs Using Mesh Network. IEEE Access. 2022. vol. 10. pp. 115295–115306. DOI: 10.1109/ACCESS.2022.3218673.
25. Muslimov T. Cooperative Circumnavigation with Robust Vector Field Guidance for Multiple UAVs in Unknown Wind Environments. J. Intell. Robot. Syst. 2023. vol. 109. no. 84. DOI: 10.1007/s10846-023-02000-3.
26. Muslimov T.Z. Metody i algoritmy gruppovogo upravlenija bespilotnymi letatel'nymi apparatami samoletnogo tipa [Methods and algorithms for formation control of fixed wing unmanned aerial vehicles]. Sistemnaya Inzheneriya i Informacionny'e Texnologii (SIIT) [Systems Engineering and Information Technologies]. 2024. vol. 6. no. 1(16). pp. 3–15. (In Russ.).
27. Lafmejani A.S., Farivarnejad H., Sorkhabadi M.R., Zahedi F., Doroudchi A., Berman S. Collision-Free Velocity Tracking of a Moving Ground Target by Multiple Unmanned Aerial Vehicles. The 4th International Symposium on Swarm Behavior and Bio-Inspired Robotics. 2021.
28. Peters S.C., Bobrow J.E., Iagnemma K. Stabilizing a vehicle near rollover: An analogy to cart-pole stabilization. IEEE International Conference on Robotics and Automation. 2010. pp. 5194–5200. DOI: 10.1109/ROBOT.2010.5509367.
29. Beard R.W., McLain T.W. Small unmanned aircraft: Theory and practice. Princeton and Oxford: Princeton University Press. 2012. 320 p.

Muslimov Tagir — Ph.D., Senior researcher, Ufa University of Science and Technology (UUST). Research interests: robotics, control theory, autonomous multi-robot systems. The number of publications — 25. tagir.muslimov@gmail.com; 12, Karl Marx St., 450008, Ufa, Russia; office phone: + 7(347)229-9616.

Acknowledgements. This work was supported by the Ministry of Science and Higher Education of the Russian Federation (Agreement No. 075-15-2021-1016).

УДК 681.5 **DOI** 10.15622/ia.24.1.4

Т.З. Муслимов

ПРЕДОТВРАЩЕНИЕ СТОЛКНОВЕНИЙ ПРИ КРУГОВОМ ДВИЖЕНИИ ГРУППЫ ДРОНОВ САМОЛЕТНОГО ТИПА НА ОСНОВЕ ВРАЩАТЕЛЬНОЙ МОДИФИКАЦИИ ИСКУССТВЕННОГО ПОТЕНЦИАЛЬНОГО ПОЛЯ

Муслимов Т.З. **Предотвращение столкновений при круговом движении группы дронов самолетного типа на основе вращательной модификации искусственного потенциального поля.**

Аннотация. При согласованном круговом движении группы автономных беспилотных летательных аппаратов (БПЛА или дронов) важно обеспечить предотвращение столкновений между ними. Характерная ситуация возникает в том случае, если один из дронов круговой формации должен обогнать впереди летящего. Причина необходимости такого обгона может заключаться в заданной геометрии формации БПЛА, когда эта конфигурация заданного взаимного положения дронов поменялась по какой-либо причине. При этом ограниченная маневренность БПЛА именно самолетного требует учета особенностей их динамики при синтезе алгоритма предотвращения столкновений. Здесь также играет роль невозможность падения воздушной скорости БПЛА самолетного типа ниже определенного минимального значения. В данной статье предлагается использовать подход на основе вихревых векторных полей, которые по сути являются вращательной модификацией метода искусственного потенциального поля (APF). При этом круговое движение обеспечивается разработанным в предыдущих наших работах алгоритмом следования вдоль линии пути. В итоге был предложен алгоритм предотвращения столкновений, который работает эффективно, сохраняя согласованное круговое движение автономной формации дронов без излишних разворотов. Данный алгоритм был назван «Artificial Potential Field for Circular Motion» (сокращенно APFfCM). С помощью прямого метода Ляпунова показано, что траектории системы формации обладают равномерной ограниченностью при использовании предлагаемого алгоритма управления. За счет ограниченности кандидата на функцию Ляпунова при этом гарантировано, что не произойдет события столкновения между дронами. Таким образом цель управления по обеспечению согласованного кругового движения без столкновений для автономной группы дронов самолетного типа достигается. Эффективная работа предлагаемого алгоритма продемонстрирована на моделях БПЛА самолетного типа («летающее крыло») в среде MATLAB/Simulink. Эти модели обладают как полной нелинейной динамикой, так и реализацией настроенных автопилотов, стабилизирующих угловое и траекторное движение.

Ключевые слова: предотвращение столкновений, группы дронов, система из нескольких БПЛА, метод искусственного потенциального поля, вихревое векторное поле.

Литература

1. Платонов А.К., Кирильченко А.А., Колганов М.А. Метод потенциалов в задаче выбора пути: история и перспективы. Препринты Института прикладной математики им. М.В. Келдыша РАН. 2001. Препринт ИПМ № 40.
2. Khatib O. Real-Time Obstacle Avoidance for Manipulators and Mobile Robots. The international journal of robotics research. 1986. vol. 5. no. 1. pp. 90–98.

3. Bojian L., Jun F., Yunxiao Q., Aijun L. Precise Formation Control for the Multi-agent Systems Based on Tilted Potential Field with Collision Avoidance. International Conference on Guidance, Navigation and Control. Lecture Notes in Electrical Engineering. 2023. vol. 845. pp. 84–93. DOI: 10.1007/978-981-19-6613-2 _10.
4. Alhaddad M., Mironov K., Staroverov A., Panov A. Neural Potential Field for Obstacle-Aware Local Motion Planning. 2023. arxiv preprint arXiv:2310.16362. DOI: 10.48550/arXiv.2310.16362.
5. Filimonov A.B., Filimonov N.B. The Concept of Fairway in Problems of Potential Guidance of Mobile Robots. Optoelectronics, Instrumentation and Data Processing. 2022. vol. 58. no. 4. pp. 366–372. DOI: 10.3103/S8756699022040057.
6. Szczepanski R., Tarczewski T., Erwinski K. Energy Efficient Local Path Planning Algorithm Based on Predictive Artificial Potential Field. IEEE Access. 2022. vol. 10. pp. 39729–39742. DOI: 10.1109/ACCESS.2022.3166632.
7. Микишанина Е.А., Платонов П.С. Алгоритмизация управления мобильным колесным роботом в среде с препятствиями методом потенциальных полей. Мехатроника, автоматизация, управление. 2024. Т. 25. № 2. С. 93–100.
8. Xi Z., Han H., Cheng J., Lv M. Reducing Oscillations for Obstacle Avoidance in a Dense Environment Using Deep Reinforcement Learning and Time-Derivative of an Artificial Potential Field. Drones. 2024. vol. 8. no. 3. DOI: 10.3390/drones8030085.
9. De Medio C., Nicolò F., Oriolo G. Robot Motion Planning Using Vortex Fields. New Trends in Systems Theory. Progress in Systems and Control Theory. Boston: Birkhäuser Boston. 1991. vol. 7. pp. 237–244.
10. De Medio C., Oriolo G. Robot Obstacle Avoidance Using Vortex Fields. Advances in Robot Kinematics. Vienna: Springer Vienna. 1991. pp. 227–235. DOI: 10.1007/978-3-7091-4433-6 _26.
11. De Luca A., Oriolo G. Local incremental planning for nonholonomic mobile robots. Proc. IEEE Int. Conf. Robot. Autom. 1994. pp. 104–110. DOI: 10.1109/ROBOT.1994.351003.
12. Martis W.P., Rao S. Cooperative Collision Avoidance in Mobile Robots using Dynamic Vortex Potential Fields. 9th Int. Conf. Autom. Robot. Appl. (ICARA 2023). 2023. pp. 60–64. DOI: 10.1109/ICARA56516.2023.10125851.
13. Choi D., Lee K., Kim D. Enhanced Potential Field-Based Collision Avoidance for Unmanned Aerial Vehicles in a Dynamic Environment. AIAA Scitech 2020 Forum. 2020. DOI: 10.2514/6.2020-0487.
14. Choi D., Kim D., Lee K. Enhanced Potential Field-Based Collision Avoidance in Cluttered Three-Dimensional Urban Environments. Appl. Sci. 2021. vol. 11. no. 22. DOI: 10.3390/app112211003.
15. Choi D., Chhabra A., Kim D. Intelligent cooperative collision avoidance via fuzzy potential fields. Robotica. 2022. vol. 40. no. 6. pp. 1919–1938. DOI: 10.1017/S0263574721001454.
16. Batinovic A., Goricanec J., Markovic L., Bogdan S. Path Planning with Potential Field-Based Obstacle Avoidance in a 3D Environment by an Unmanned Aerial Vehicle. International Conference on Unmanned Aircraft Systems (ICUAS). 2022. pp. 394–401. DOI: 10.1109/ICUAS54217.2022.9836159.
17. Goricanec J., Milas A., Markovic L., Bogdan S. Collision-Free Trajectory Following With Augmented Artificial Potential Field Using UAVs. IEEE Access. 2023. vol. 11. pp. 83492–83506. DOI: 10.1109/ACCESS.2023.3303109.
18. Szczepanski R. Safe Artificial Potential Field – Novel Local Path Planning Algorithm Maintaining Safe Distance From Obstacles. IEEE Robot. Autom. Lett. 2023. vol. 8. no. 8. pp. 4823–4830. DOI: 10.1109/LRA.2023.3290819.

19. Su Y.-H., Bhowmick P., Lanzon A. A Fixed-time Formation-containment Control Scheme for Multi-agent Systems with Motion Planning: Applications to Quadcopter UAVs. IEEE Transactions on Vehicular Technology. 2024. vol. 73. no. 7. pp. 9495–9507. DOI: 10.1109/TVT.2024.3382489.
20. Muslimov T. Curl-Free Vector Field for Collision Avoidance in a Swarm of Autonomous Drones. Lecture Notes in Computer Science. Interactive Collaborative Robotics (ICR 2023). 2023. vol. 14214. pp. 369–379.
21. Muslimov T., Kozlov E., Munasypov R. Drone Swarm Movement without Collisions with Fixed Obstacles Using a Hybrid Algorithm Based on Potential Functions. International Russian Automation Conference (RusAutoCon). 2023. pp. 781–785.
22. Gao Y., Bai C., Fu R., Quan Q. A non-potential orthogonal vector field method for more efficient robot navigation and control. Rob. Auton. Syst. 2023. vol. 159. DOI: 10.1016/j.robot.2022.104291.
23. Park C., Cho N., Lee K., Kim Y. Formation Flight of Multiple UAVs via Onboard Sensor Information Sharing. Sensors. 2015. vol. 15. no. 7. pp. 17397–17419.
24. Kim S., Cho H., Jung D. Circular Formation Guidance of Fixed-Wing UAVs Using Mesh Network. IEEE Access. 2022. vol. 10. pp. 115295–115306. DOI: 10.1109/ACCESS.2022.3218673.
25. Muslimov T. Cooperative Circumnavigation with Robust Vector Field Guidance for Multiple UAVs in Unknown Wind Environments. J. Intell. Robot. Syst. 2023. vol. 109. no. 84. DOI: 10.1007/s10846-023-02000-3.
26. Муслимов Т.З. Методы и алгоритмы группового управления беспилотными летательными аппаратами самолетного типа. Системная инженерия и информационные технологии. 2024. Т. 6. № 1(16). С. 3–15.
27. Lafmejani A.S., Farivarnejad H., Sorkhabadi M.R., Zahedi F., Doroudchi A., Berman S. Collision-Free Velocity Tracking of a Moving Ground Target by Multiple Unmanned Aerial Vehicles. The 4th International Symposium on Swarm Behavior and Bio-Inspired Robotics. 2021.
28. Peters S.C., Bobrow J.E., Iagnemma K. Stabilizing a vehicle near rollover: An analogy to cart-pole stabilization. IEEE International Conference on Robotics and Automation. 2010. p. 5194–5200. DOI: 10.1109/ROBOT.2010.5509367.
29. Beard R.W., McLain T.W. Small unmanned aircraft: Theory and practice. Princeton and Oxford: Princeton University Press. 2012. 320 p.

Муслимов Тагир Забирович — кандидат техн. наук; старший научный сотрудник Уфимского университета науки и технологий (УУНиТ). Область научных интересов: робототехника, теория управления, автономные мультироботные системы. Число научных публикаций — более 25. ORCID: https://orcid.org/0000-0002-9264-529X Email: tagir.muslimov@gmail.com; ФГБОУ ВО «УУНиТ», ул. К.Маркса, д. 12, г. Уфа, 450008, РФ.

Поддержка исследований. Работа выполнена при поддержке Министерства науки и высшего образования Российской Федерации (Соглашение № 075-15-2021-1016).